Eur. Phys. J. E (2018) **41**: 66
DOI 10.1140/epje/i2018-11672-1

THE EUROPEAN PHYSICAL JOURNAL E

Regular Article

Nonequilibrium processes in meta-stable media*

N.N. Smirnov[1,2,4,a], O.G. Penyazkov[3,4], K.L. Sevrouk[3], V.F. Nikitin[1,4], L.I. Stamov[1,2,4], and V.V. Tyurenkova[2,4]

[1] Moscow Lomonosov State University, Moscow 119992, Russia
[2] Scientific Research Institute for System Analysis of Russian Academy of Sciences, Moscow 117218, Russia
[3] Lykov's Heat and Mass Transfer Institute of National Academy of Science of Belarus, P.Brovki 15, Minsk, Belarus
[4] LLC "Center for Numerical Modeling", Moscow, Zelenograd 124482, Russia

Received 23 July 2017 and Received in final form 13 October 2017
Published online: 24 May 2018

Abstract. Meta-stable systems are those staying in the local equilibrium state: being slightly deviated from it they return to the equilibrium, but in case deviation surpasses a critical value those systems fall down to another equilibrium state. Chemically reacting gaseous mixture provides a typical example of a meta-stable system. The paper is aimed at numerical and experimental investigation of detonation initiation in hydrogen-air mixtures due to focusing of a shock wave reflected inside a wedge. Both numerical and experimental investigations were conducted. Comparison of numerical and experimental results made it possible to validate the developed 3D transient mathematical model of chemically reacting gas mixture flows incorporating hydrogen-air mixtures. Kinetic schemes and turbulence models were improved based on comparison of numerical and experimental results. Several different flow scenarios manifest in the reflection of shock waves all being dependent on the incident shock wave intensity: reflection of the shock wave with lagging behind the combustion zone, formation of a detonation wave in reflection and focusing, and intermediate transient regimes.

1 Introduction

Combustible systems present typically in meta-stable states, which means that, being slightly heated, they return in time to ambient temperature due to heat losses. While being heated to a definite extent such systems give birth to self-sustained combustion waves, which convert the gaseous mixture from one local equilibrium state of initial chemical species to final equilibrium state of reaction products. This transition is accompanied by chemical energy release giving support for the self-sustained propagation of a chemical reaction zone. The process is generally named combustion. As it was known since the beginning of the 20th century, combustion in gaseous mixtures could take place in two different modes: deflagration and detonation. Deflagration is a subsonic combustion mode, which serves as the basis for the working cycle of all the combustion engines now. Detonation is a supersonic combustion mode, which was considered to be harmful for engines due to intense loads. The detonation combustion mode has definite exceptional properties as compared with the classical deflagration mode used in modern engines. These differences are: extraordinary higher rates of flame propagation (four orders of magnitude higher), higher pressure and temperature values in the reaction zone, minimal entropy production for the Chapman-Jouget regime. Unsteady-state transition processes between the two combustion modes are possible. The control of the detonation onset is necessary in perspective pulse detonation engines using hydrogen-air mixtures in the working cycle, which are under development now. Hydrogen fuel is a very perspective fuel making the engine exhaust much cleaner than that for hydrocarbon combustion [1,2]. Chemical kinetics for hydrogen-air mixtures combustion are well developed [3–8]. The advantages of a constant volume combustion cycle as compared to constant pressure combustion in terms of thermodynamic efficiency has focused the search for advanced propulsion on detonation engines [9–11]. Temperature in a constant volume cycle could be, generally, higher than that in a constant pressure cycle, which could lead to an increase of NO_x production rate. However, the NO_x production rate is still slow as compared with other reaction stages. Numerical simulations of pulse detonation engines operation aimed at increasing their efficiency and developing control strategies consume

* Contribution to the Topical Issue "Non-equilibrium processes in multicomponent and multiphase media" edited by Tatyana Lyubimova, Valentina Shevtsova, Fabrizio Croccolo.

[a] e-mail: ebifsun1@mech.math.msu.su
(corresponding author)

much time and computational recourses. Parallel computing technologies and developing effective schemes aim at reducing the simulation time [12–18]. The thermodynamic efficiency of the Chapman-Jouget detonation as compared with slow combustion modes is due to the minimal entropy of the exhaust jet [11]. During the past several decades different schemes of pulse detonation engines were suggested and aimed to demonstrate that the proper utilization of the operation cycle does result in improved performance. Deflagration to detonation transition processes were studied with the goal of making this process serve as the basis for the detonation onset within a working cycle, as well as continuously working engines with rotating detonation wave were modeled [19–33]. There still exist many issues in developing this technology, which represent scientific and technological challenges. In particular, it is not clear up to now, which principle of pulse detonating cycle is more effective: co-flow or counter-flow detonation wave propagation and what cycle is preferable: pulse detonation or rotating detonation. The success in resolving these problems will determine the implementation of detonation propulsion. Extensive numerical multidimensional simulations of detonation onset and propagation are necessary in combustion chambers able to distinguish the optimal scheme for the operation cycle. Parallel computing is a powerful tool enabling to make simulations more effective and less time consuming [12–18]. However not all numerical problems allow effective parallelization. Thus problems of the effective acceleration of simulation procedures have their theoretical limits [34,35].

The aim of the present study is investigating detonation initiation at short distances by relatively weak initiators using the advantage of shock waves focusing and energy cumulation in the reflection inside a wedge. Theoretical investigations and numerical simulations will be supported by experimental studies in a shock tube.

2 Mathematical model

Equations

In order to calculate multicomponent gas dynamics with chemical reactions excluding transport phenomena effects and considering external mass and energy sources we use the following set of simultaneous equations:

$$\frac{\partial \rho_k}{\partial t} + \frac{\partial}{\partial x_j}(\rho_k u_j) = \dot{\omega}_k + \dot{M}_k; \tag{1}$$

$$\frac{\partial \rho u_i}{\partial t} + \frac{\partial}{\partial x_j}(\rho u_i u_j) + \frac{\partial p}{\partial x_i} = 0; \tag{2}$$

$$\frac{\partial}{\partial t}\left(E + \rho\frac{u^2}{2}\right) + \frac{\partial}{\partial x_j}\left(\left(E + p + \rho\frac{u^2}{2}\right)u_j\right) = \dot{Q} + \dot{Q}_M. \tag{3}$$

In eqs. (1)–(3) the index k takes values $1, \ldots, N_C$ (number of components) and the indices i, j take values 1, 2, 3 (number of dimensions); repeated indices presume summation. In total there are $N_C + 4$ differential equations in the set.

Algebraic relations

Differential equations (1)–(3) are to be complemented with three algebraic relations and algebraic representations for chemical and mass and energy sources. The first three relations will look like:

$$\begin{aligned} \rho &= \sum_{k=1}^{N_C} \rho_k, \\ p &= R_G T \sum_{k=1}^{N_C} \frac{\rho_k}{W_k}, \\ E &= R_G T \sum_{k=1}^{N_C} \frac{\rho_k}{W_k}(\hat{H}_k(T) - 1). \end{aligned} \tag{4}$$

Relations (4) define gas density ρ, pressure p and internal energy per unit volume E of the mixture, respectively. Other definitions are: R_G —universal gas constant, W_k —molar weight of a component and for temperature functions – $\hat{H}_k(T)$ —dimensionless enthalpy of a component encompassing the enthalpy of formation at a given temperature T_{ref} ("chemical energy"). More precisely the conception of dimensionless thermodynamic data is given in [1]. As these expressions show, in algebraic expressions here and in what follows it is often convenient to use the molar density X_k (which sometimes, especially in chemical literature, is called "concentration") instead of the partial component density ρ_k:

$$X_k = \frac{\rho_k}{W_k}. \tag{5}$$

The mass source $\dot{\omega}_k$ is due to the chemical interactions present in the system of gases. The mass source $\dot{M}_k$ results from the external source outcome. The source $\dot{Q}_M$ in the energy equation is a total income of energy carried with the external mass $\dot{M}_k$; the source $\dot{Q}$ in the energy equation denotes extra energy income from the external source. The thermal energy source implying chemical reactions inside the system is absent in this model because energy E already encompasses the chemical energy of each component. External sources are not directly linked chemical interactions inside the system; they aim to inject mass and energy in the gas mixture from the outside for ignition and movement excitation. In our problem setup they explicitly depend on time and location.

Chemical sources $\dot{\omega}_k$ for most systems take a complicated form; they can be expressed depending on temperature T and set of the molar densities $\mathbf{X} = \{X_k\}$; the sum of these sources equals zero due to the law of mass conservation in chemical reactions:

$$\dot{\omega} = W_k \hat{\omega}_k(T, \mathbf{X}), \qquad \sum_{k=1}^{N_C} \dot{\omega}_k = 0. \tag{6}$$

There also exist more precise laws of chemical interactions (law of mass conservation for each element), which are taken into account in the kinetic mechanism and can be considered in the numerical realization of the model for the

Table 1. Chemical kinetics mechanism. Units: cm, s, mol, K.

1.	O_2+H=OH+O	$6.06 \cdot 10^{14} \cdot T^{-0.097} \cdot \exp(-7560/T)$
2.	H_2+O=OH+H	$5.06 \cdot 10^{4} \cdot T^{2.67} \cdot \exp(-3163/T)$
3.	H_2+OH=H_2O+H	$2.17 \cdot 10^{8} \cdot T^{1.52} \cdot \exp(-9650/T)$
4.	OH+OH=H_2O+O	$3.35 \cdot 10^{4} \cdot T^{2.42} \cdot \exp(+969.5/T)$
5.	H+H+M_1=H_2+M_1[2]	$1.80 \cdot 10^{18} \cdot T^{-1}$
6.	O+O+M_1=O_2+M_1	$2.90 \cdot 10^{17} \cdot T^{-1}$
7.	H+OH+M_1=H_2O+M_1	$2.20 \cdot 10^{22} \cdot T^{-2}$
8.	H+O_2+M_1=HO_2+M_1	$2.30 \cdot 10^{18} \cdot T^{-0.8}$
9.	HO_2+H=OH+OH	$1.50 \cdot 10^{14} \cdot \exp(-505.0/T)$
10.	HO_2+H=H_2+O_2	$1.05 \cdot 10^{14} \cdot \exp(-1029/T)$
11.	HO_2+H=H_2O+O	$3.00 \cdot 10^{13} \cdot \exp(-866.0/T)$
12.	HO_2+O=OH+O_2	$1.80 \cdot 10^{13} \cdot \exp(+204.5/T)$
13.	HO_2+OH=H_2O+O_2	$6.00 \cdot 10^{13}$
14.	HO_2+HO_2=H_2O_2+O_2	$2.50 \cdot 10^{11} \cdot \exp(+625.5/T)$
15.	OH+OH+M_1=H_2O_2+M_1	$3.25 \cdot 10^{22} \cdot T^{-2}$
16.	H_2O_2+H=H_2+HO_2	$1.70 \cdot 10^{12} \cdot \exp(-1888/T)$
17.	H_2O_2+H=H_2O+OH	$1.00 \cdot 10^{13} \cdot \exp(-1804/T)$
18.	H_2O_2+O=OH+HO_2	$2.80 \cdot 10^{13} \cdot \exp(-3223/T)$
19.	H_2O_2+OH=H_2O+HO_2	$5.40 \cdot 10^{12} \cdot \exp(-505.2/T)$
20.	O+H+M_2=OH+M_2[3]	$4.71 \cdot 10^{18} \cdot T^{-1}$

calculation simplification and precision improvement. A general form of chemical sources is quite complicated and includes members which are nonlinear for each argument; the common view is

$$\omega_r = M_r(\mathbf{X}) \times \left[k_{F,r}(M_r, T) \prod_j X_j^{\alpha_{r,j}} - k_{R,r}(M_r, T) \prod_j X_j^{\beta_{r,j}} \right], \quad (7)$$

where ω_r is the speed (intensity) of the reaction r, $\nu_{r,k}$ is an algebraic stoichiometric coefficient of a component k in the reaction r, M_r is a third bodies influence coefficient (those which don't change) in the reaction r, which equals 1 when this influence is absent, $k_{F,r}$ is a speed coefficient of a forward reaction, usually depending solely on temperature, but for some ("out-of-order") reactions also of M_r, $k_{B,r}$ is a speed coefficient of the backward reaction, $\alpha_{r,k}$ are the powers of components in the forward reaction (usually, but not always nonzero only for incoming components) $\beta_{r,k}$ are the powers of components in the backward reaction.

Dependencs $\hat{H}_k(T)$ are often expressed as polynomials with different coefficients for different components.

Details of the detonation onset simulation peculiarities can be found in [11,19,20].

3 Numerical calculation conditions

Two different shock-capturing methods were tested with the same parameters:

1) Explicit second order in space and time method based on the MUSCL-interpolation of variables on a face at a convective flux calculation. Interpolation direction choice and pressure interpolation were performed by means of the AUSMP method [13–18]. The method was implemented on a regular grid containing equal elements (rectangular parallelepipeds) connected generally in arbitrary topology. The source code was written in C. Parallel execution support was implemented using OpenMP library.
2) Explicit second order in space and time scheme based on the Kurganov-Tadmor method. The method was implemented on a regular grid (rectangular parallelepipeds). Source codes were written in FORTRAN.

Components list and kinetics mechanism

Hydrogen, oxygen and nitrogen were merely the components of the initial mixture. During combustion besides the final product —water vapor— a manifold of intermediate products (radicals) is generated and at high enough temperature remains in the mixture. The following components were used:

$$\{H_2O, OH, H, O, HO_2, H_2O_2; O_2, H_2, N_2\}.$$

In calculations we used the kinetic mechanism of hydrogen combustion without nitrogen oxides formation (those reactions are reasonably slow to influence detonation and combustion and usually are calculated *a posteriori*). As a basis we took the Maas-Warnatz mechanism [8], which was then developed in [9,10]. The modified mechanism is shown in table 1.

In table 1 the following notations are used:

1) $M_1 = 6.5 \cdot [H_2O] + 0.35 \cdot [O_2] + 0.35 \cdot [N_2] + 1.0 \cdot [X]$. Molar density of components in [mol/cm^3], [X] the sum of molar densities of other components.
2) $M_2 = 12.0 \cdot [H_2O] + 12.0 \cdot [H_2O_2] + 2.5 \cdot [H_2] + 1.0 \cdot [X]$.

Table 1 does not contain reactions responsible for NO_x formation though combustion takes place in the presence of nitrogen. The NO_x production rate is too slow as compared with other reaction stages for hydrogen-air combustion. The flame temperature for hydrogen-air combustion is too low to guarantee a comparable NO_x production reaction rate. Thus a general method of taking into account NO_x is the following: first, reactions of hydrogen combustion are taken into account and a new mixture composition and temperature are developed; second, NO_x production under the obtained conditions is simulated. NO_x concentration could reach no more than 0, 1%, which is enormous for a pollutant, but it is negligible in terms of affecting the hydrogen oxidation reactions in a detonation wave.

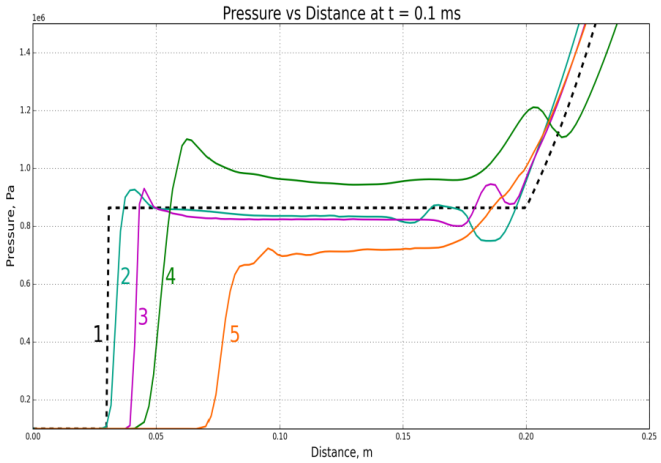

Fig. 1. Comparison of numerical results with the exact solution of the self-similar problem on the discontinuity evolution. 1: exact self-similar solution; 2: numeric solution scheme 2 hybrid systems; 3: numeric solution scheme 1 universal systems; 4, 5: solutions obtained by different modifications of commercial codes.

4 Testing the developed codes

Sod tests

As a model objective for the verification of CFD solvers were picked Sod problems [36,37], in which the result of the numerical solution of a one-dimensional Riemann problem is compared with the analytical solution obtained by u-p diagrams method. A brief description of the setup is as follows: the gas is placed in the tube and divided by a partition (diaphragm). From the left of the diaphragm the state of the gas is characterized by pressure p_L, density ρ_L and speed u_L; similarly, the options to the right of the partition are p_R, ρ_R, u_R. In the beginning of the computation the partition is removed, and we monitor the evolution of discontinuity present in the initial data. The mixture in these tests is nonreactive. Two tests were conducted.

The detailed results described in [38] showed that the difference between numerical simulations and exact solution does not exceed 3%.

Detonation initiation tests for reactive mixture

In order to assess performance of both methods on the objectives with reactive fluids we considered the following setup. As in the tests above we have a tube which is separated in two halves with a diaphragm, but this time the gas on the left side of the diaphragm is reactive (oxygen-hydrogen-nitrogen mixture with mass fractions $[H_2] : [O_2] : [N_2] = 2 : 1 : 1$) and at low pressure (1 bar) and on the other side it is nonreactive (N_2) and at high pressure (80 bar). The initial temperature in the reactive gas is 700 K and in nitrogen it is of 1500 K. Both reactive and nonreactive gases before the start of the test are resting. At the beginning of the calculation the diaphragm is removed and the emerging shock wave, which propagates through the reactive mixture, initiates detonation.

The results of this test were also compared with the exact solution obtained by the u-p diagrams method (fig. 1).

A descent coincidence between numerical solutions and the exact one was demonstrated [38]. The Kurganov-Tadmor method appears to have its detonation wave propagating further, than for MUSCL-AUSMP. Most likely this is not linked with the different speed of detonation propagation calculated on both methods but with the difference in the ignition delay. All the codes demonstrate a discrepancy with the analytical solution in the zone of contact between combustible and inert mixtures. This discrepancy is understandable, because an analytical self-similar solution was obtained based on the assumption of the instantaneous detonation onset on entering the shock wave into the combustible mixture. In reality, the ignition delay time leads to the emergence of an unsteady transition period, which becomes longer on decreasing the intensity of the shock wave.

The effect of the grid resolution on the detonation wave simulation for both schemes was studied in [39]. The resolution within which the flow structure and wave velocity did not change after 8-times increase of the number of computational cells, was assumed grid independent. All the results present in this paper were obtained using grid-independent simulations.

5 Results of numerical simulations

5.1 Computation domain

The problem simulating processes in the final section of the shock tube is considered. The shock tube diameter was 76 mm, length: 720 mm. (fig. 2). The tube is filled in

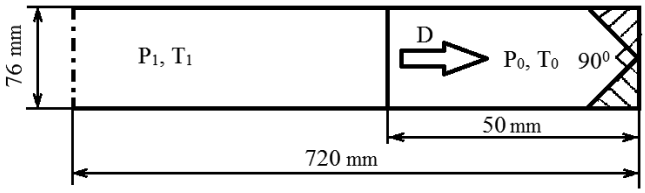

Fig. 2. Computational domain.

Table 2. Initial conditions for test simulations and Chapman-Jouget parameters for the mixture.

No.	1	2	3
	WEDGE02R	WEDGE19Q	WEDGE08P
T_0, K	294	293	295
P_0, bar	0.28	0.37	0.12
T, K	593	421	559
P, bar	1.85	1.13	0.66
v_x, m/s	672	362	617
D, m/s	969	675	915
V_{CH}, m/s	1933	1942	1908
P_{CH}, bar	14.47	12.36	5.35
T_{CH}, K	2978	2913	2879

with hydrogen-air mixture. A special end section was installed into the tube providing a wedge cavity with the opening angle 90°. A plane shock wave is reflecting from the wedge, and processes accompanying focusing are regarded. The tube is a circular cylinder with an axial symmetry, the end section incorporating wedge has a rectangular cross-section. This configuration was chosen for studying reflection in a wedge. (The cone reflection was investigated in [40]).

The tube initially is filled in with a combustible mixture at a temperature T_0 and pressure P_0. The shock wave velocity is D and the parameters of compressed gas are T, P and V_x. Table 2 presents theoretically calculated parameters for the Chapman-Jouget detonation for the test cases considered: temperature (T_{CH}) and pressure (P_{CH}), as well as detonation wave velocity (V_{CH}).

5.2 Simulation results obtained by scheme 1: MUSCL, AUSM, K-Omega

5.2.1 Initial conditions and coordinate system

The coordinate system $Oxyz$ has its origin at the axis of the cylindrical tube. Then the domain can be described by the following inequalities:

$$x \geq 0, \quad x \leq L, \quad y^2 + z^2 \leq R^2, \tag{8}$$

$$x > L - R : |y| \leq (L - x). \tag{9}$$

The initial states of the gaseous mixture

$$\begin{aligned} P_0, T_0 \quad & \text{are varied,} \\ [\mathrm{H_2}] : [\mathrm{O_2}] : [\mathrm{N_2}] &= 2 : 1 : 3.76, \\ \mathbf{u}_{ini} &= \{0, 0, 0\}. \end{aligned} \tag{10}$$

State (10) was near the right-hand end of the tube. The state of gas behind the shock wave was described by the following parameters:

$$\begin{aligned} P_1, T_1 \quad & \text{are varied,} \\ [\mathrm{H_2}] : [\mathrm{O_2}] : [\mathrm{N_2}] &= 2 : 1 : 3.76, \\ \mathbf{u}_0 &= \{U_0, 0, 0\}. \end{aligned} \tag{11}$$

At $t = 0$ the position of the shock wave is $x = x_0$, so that for $x > x_0$ the initial state is described by (10), and for $x \leq x_0$ the initial state is described by (11). $x_0 = 0.67\,\mathrm{m}$. The initial conditions variation corresponds to that in experiments.

By taking into account turbulence the following initial parameters for the turbulent kinetic energy and Reynolds number were adopted for all the computational domain:

$$\begin{aligned} K_{ini} &= 0.1\,\mathrm{J/kg}, \\ \mathrm{Re}_T = \frac{\nu_T}{\nu} &= \frac{K_{ini}}{\omega_{ini}} \cdot \frac{\rho(X_{ini})}{\mu(T_{ini}, X_{ini})} = 0.1. \end{aligned} \tag{12}$$

5.2.2 Onset of detonation on focusing in the reflection from a wedge cavity

Figures 3–5 illustrate the distribution of different flow parameters for successive time moments in cross-section planes: meridional and orthogonal, for numerical experiments WEDGE02R. The section $x \in [0.52, 0.72]\,\mathrm{m}$ is shown. Figure 3 illustrates the pressure distribution in the meridional plane Oxy, the characteristic time is shown below each figure, mapping colors are shown before the caption.

It is seen from fig. 3 that on focusing the reflected shock waves the onset of detonation takes place. At time 0.015 ms the shock wave reaches the wedge and the reflection from its internal surface begins, at time 0.036 ms the reflection continues and becomes well visible at 0.05 ms. At time 0.06 ms the wave is focused near the axis, its intensity increases up to 30 bars, and at 0.065 ms a detonation wave is born in the peak of the wedge, while the intensity of the focused wave decreases due to its divergence from the axis. At times 0.08–0.095 ms the detonation wave propagates from the wedge in the medium with nonuniform parameters due to shock wave focusing, at 0.10 ms it leaves the wedge and for successive times 0.115–0.175 ms transverse waves are formed behind the detonation wave, which collide and interact in the reaction products. The leading front of the detonation wave is seen at times 0.155–0.175 ms, which was plane before, it becomes curved, and the detonation propagates faster near the walls than near the axis. This effect is due to the turbulent boundary layer, wherein gas velocity is practically zero, while near

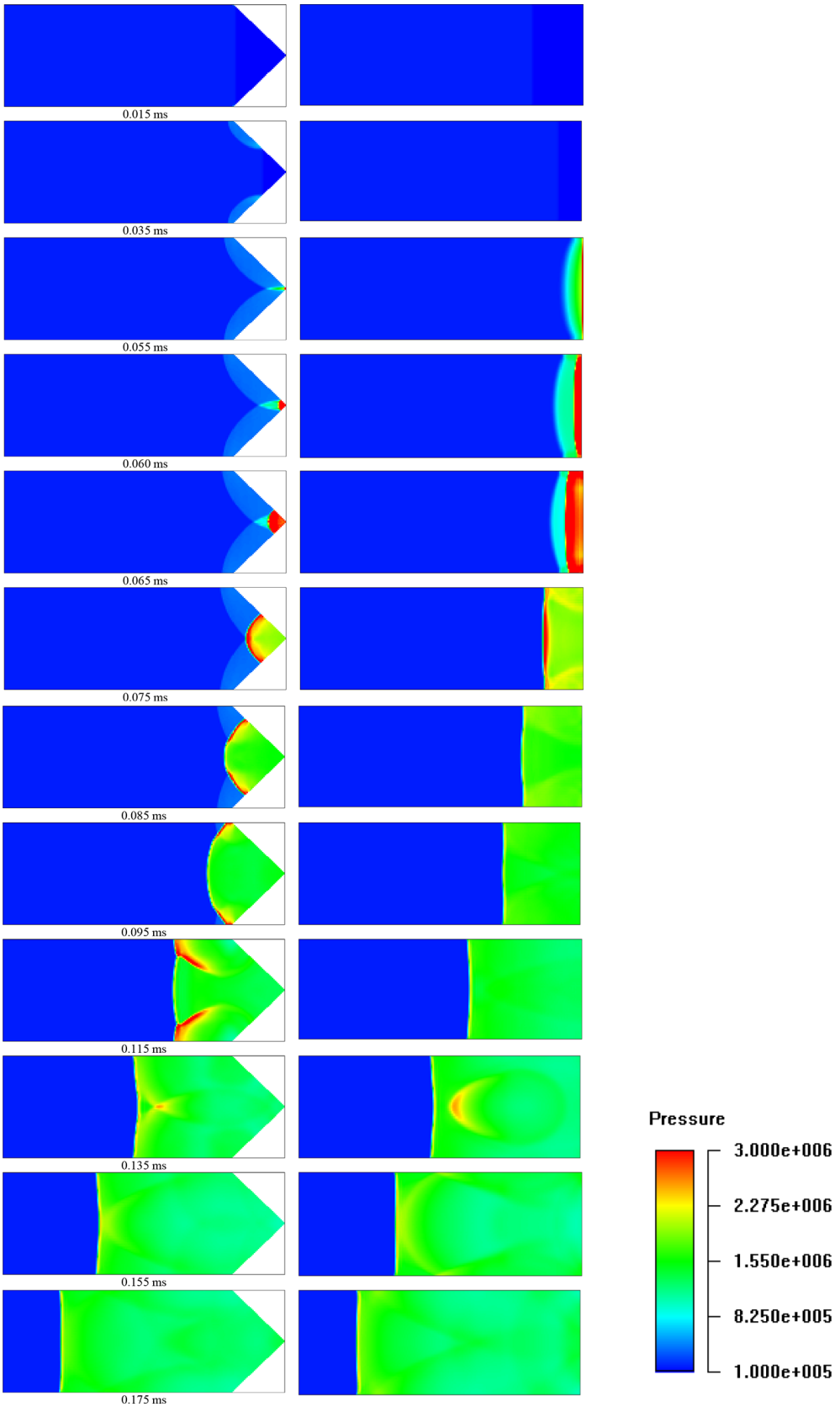

Fig. 3. Pressure fields in (Pa) on focusing shock wave and detonation onset in the reflection from a wedge surface. Meridian cross-sections Oxy (left) and Oxz (right); version WEDGE02R.

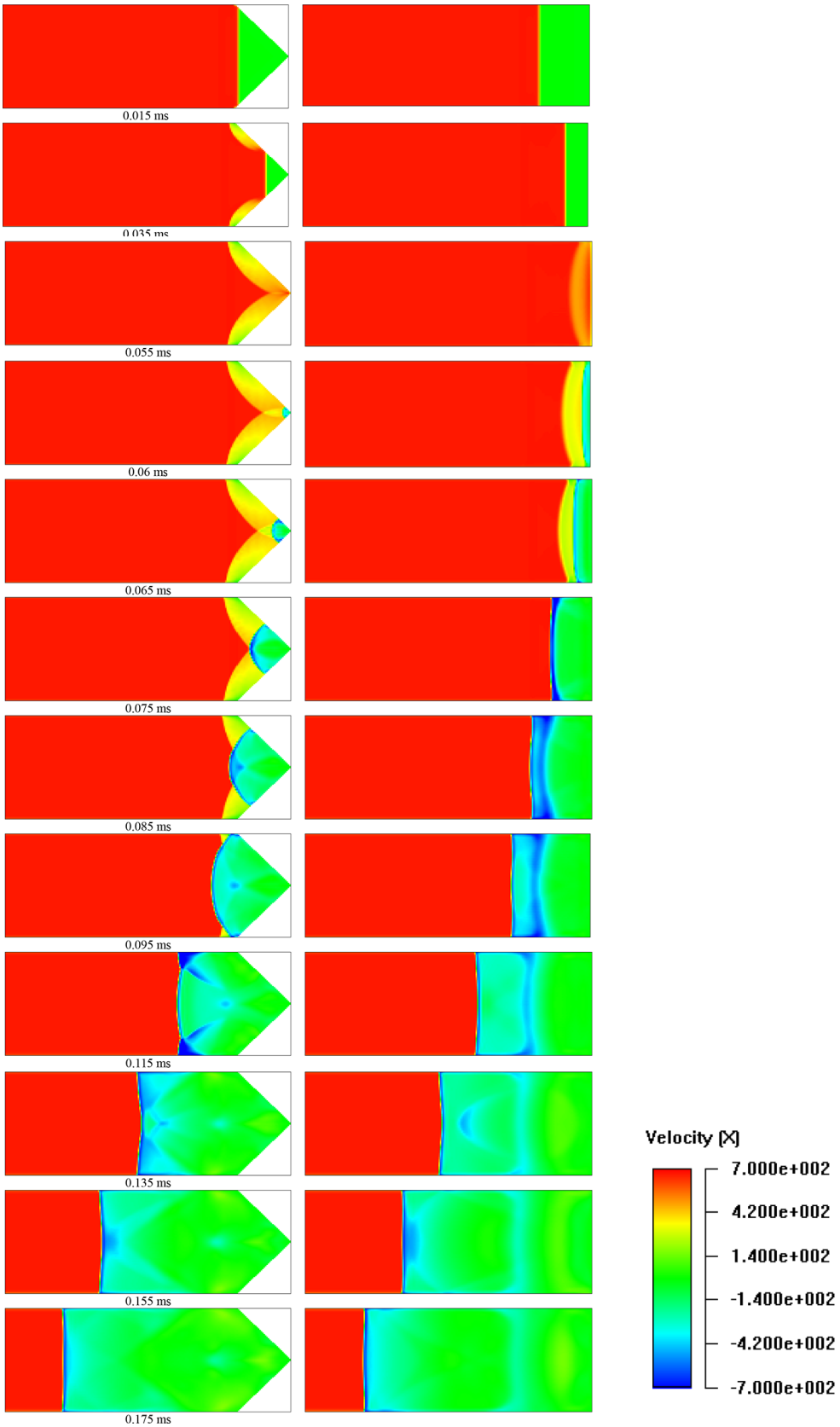

Fig. 4. Axial velocity fields in (m/s) on focusing shock wave and detonation onset in the reflection from a wedge surface. Meridian cross-sections Oxy (left) and Oxz (right); version WEDGE02R.

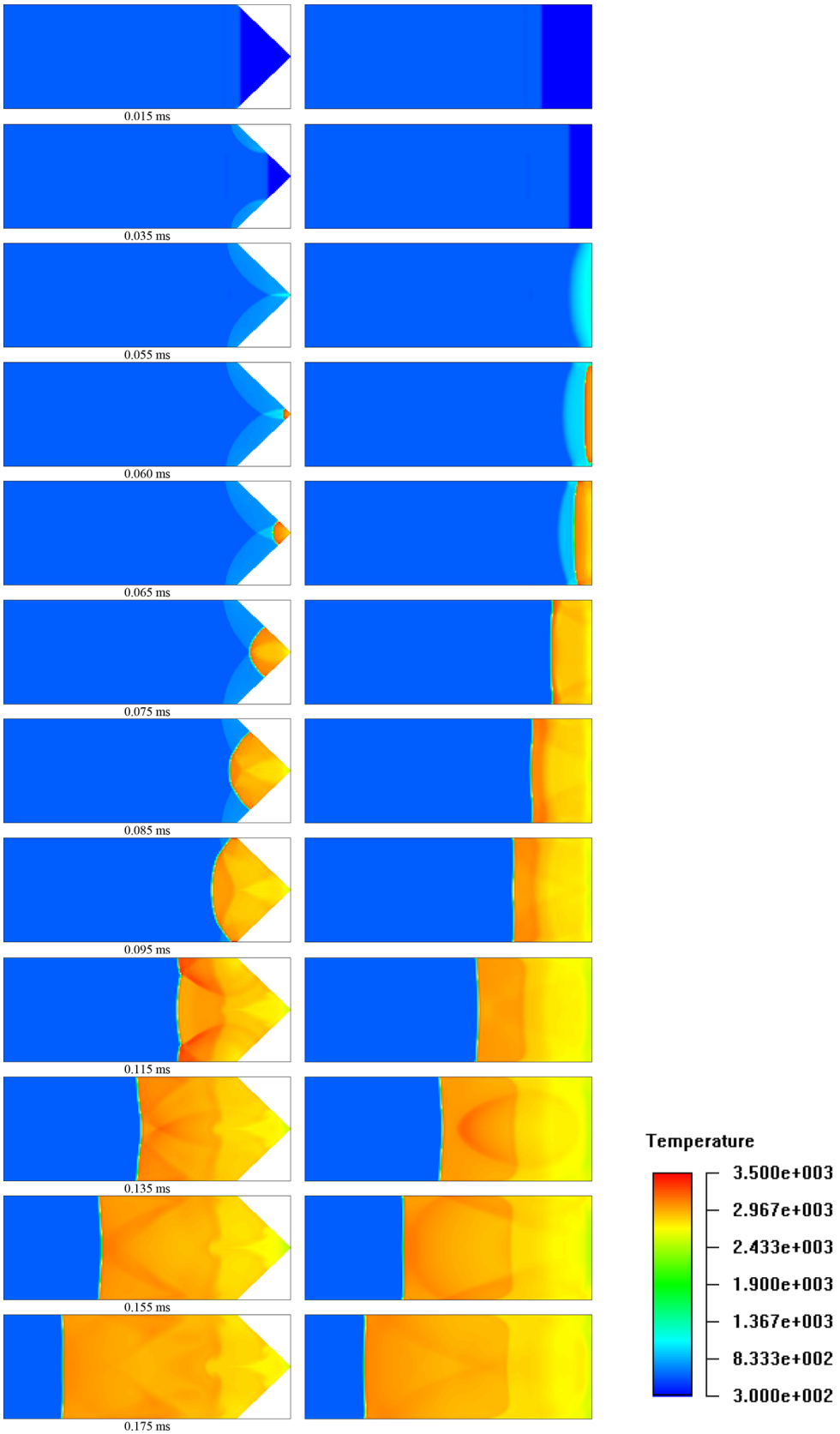

Fig. 5. Temperature evolution in focusing of a reflected detonation wave inside a wedge depicted in the Oxy plane (left) and Oxz plane (right); version WEDGE02R.

the axis detonation propagates in a high velocity opposing flow. Thus the mean velocity of the detonation complex in simulations as well as in experiment is a little bit higher than the estimated Chapman-Jouget velocity. For numerical experiments with switched-off viscosity the detonation wave velocity in reflection coincides with the theoretical Chapman-Jouget value.

In fig. 4 the velocity component in the Ox direction is shown in Oxy and Oxz meridional planes. Negative velocity values correspond to the motion from the right to the left. It is seen from fig. 4 that the time moment 0.06 ms is characterized by a sharp increase of the flow velocity in the tip of the cone.

At time 0.065 ms the onset of detonation is observed in the tip of the wedge. Then the detonation wave propagates outside the wedge.

Figure 5 illustrates the temperature distribution in Oxy and Oxz planes. The burnt gas is characterized by a temperature of 1600–2000 K.

As is seen from fig. 5, initially the temperature field tracks the position of shock waves. At time 0.055 ms shock wave focusing took place, but the combustible mixture was not ignited. At time 0.06 ms ignition in the tip of the wedge is noticeable, the temperature there increases up to 3500 K for a short time. Then the temperature behind the detonation wave decreases to 2500–2900 K.

The molar concentration (or volume share) of the OH radical is shown in fig. 6. This radical was detected in experiments in order to track the combustion zone. Contrary to all previous diagrams the logarithmic scale is used for depicting the value of this concentration, because it can vary by several orders of magnitude. Before time 0.055 ms chemical transformations do not manifest, thus the volume share of the OH radical is not shown in the figure until this time.

It is seen from fig. 6 that until time 0.055 ms the mixture is not ignited, though the temperature in the tip is very high. This means that an increase of temperature before 0.06 ms is due to adiabatic heating in gas compression, but not to chemical processes.

The numerical simulations of the WEDGE20R version was performed taking into account turbulence. Figure 7 illustrates the evolution of the turbulent kinetic energy in the Oxy plane. The scale is logarithmic.

It is seen from fig. 7 that in the beginning the turbulent kinetic energy is distributed in the vicinity of the walls. On propagating the incident shock wave and its focusing near the axis (times: 0.04–0.065 ms) the turbulent energy near the walls increases. For longer times after the reflection of the detonation wave the increase of the turbulent energy near the axis is also seen.

5.3 Simulation results obtained by scheme 2: Kurganov-Tadmor

In figs. 8–18 successive stages for the process of incident shock wave reflection and focusing in a wedge are presented including the onset of a detonation wave. Figures 8–13 illustrate the distribution of parameters along the whole tube, while in figs. 14–18 the distribution of parameters in the proximity of the wedge is shown.

Figure 18 illustrates the successive stages of the incident shock wave reflection from a wedge for different initial conditions corresponding to the experiment WEDGE19Q. One can see that the focusing of shock waves leads to the formation of a reflected shock wave, but does not initiate detonation.

6 Experimental investigations

Experimental studies were performed in a shock tube with a conical cavity at the end. The reflection of shock waves of different intensity was analyzed. Pressure-time history and OH radical emission were recorded. Figure 19 presents the scheme of the measuring section of the shock tube, in which experiments on shock waves focusing were conducted. A similar geometry was used in numerical simulations. In numerical simulations gas dynamic parameters variation in the place of pressure transducers location were recorded as well. Details on the experiments can be found in [41,42].

Experimental investigations showed that depending on the incident shock wave intensity different flow scenarios could take place. For a relatively low intensity of the incident shock wave after reflection and focusing inside the cone a shock wave is formed, and some lagging behind ignition and combustion could form. For high enough incident shock intensity after its reflection and focusing inside the cone the detonation onset takes place. We will perform a comparison of experimental and numerical results for the most interesting cases of the onset of detonation in reflecting from inside a conical cavity.

7 Comparing numerical and experimental results

A comparison of numerical simulation results and experimental data is performed based on pressure records in five different places after the incident shock reflection (figs. 20–23). The method is similar to that applied in [38] for studying a symmetrical problem of reflection from the cone. Here a nonsymmetrical problem of reflection from a wedge is considered. Due to that reason the data on the numerical evolution of parameters is obtained exactly in the places of transducers' location.

A comparison of experimental data and simulations results for OH radicals is not presented. Experimental data provides an integral value along the axis and allows detecting the moment of detonation onset for the present experiments under consideration. It just testifies pressure diagrams. The coincidence of numerical and experimental data was good, as expected. The results were not provided due to triviality. A comparison could be interesting for different experiments (mild ignition), when OH and pressure graphics are not coherent.

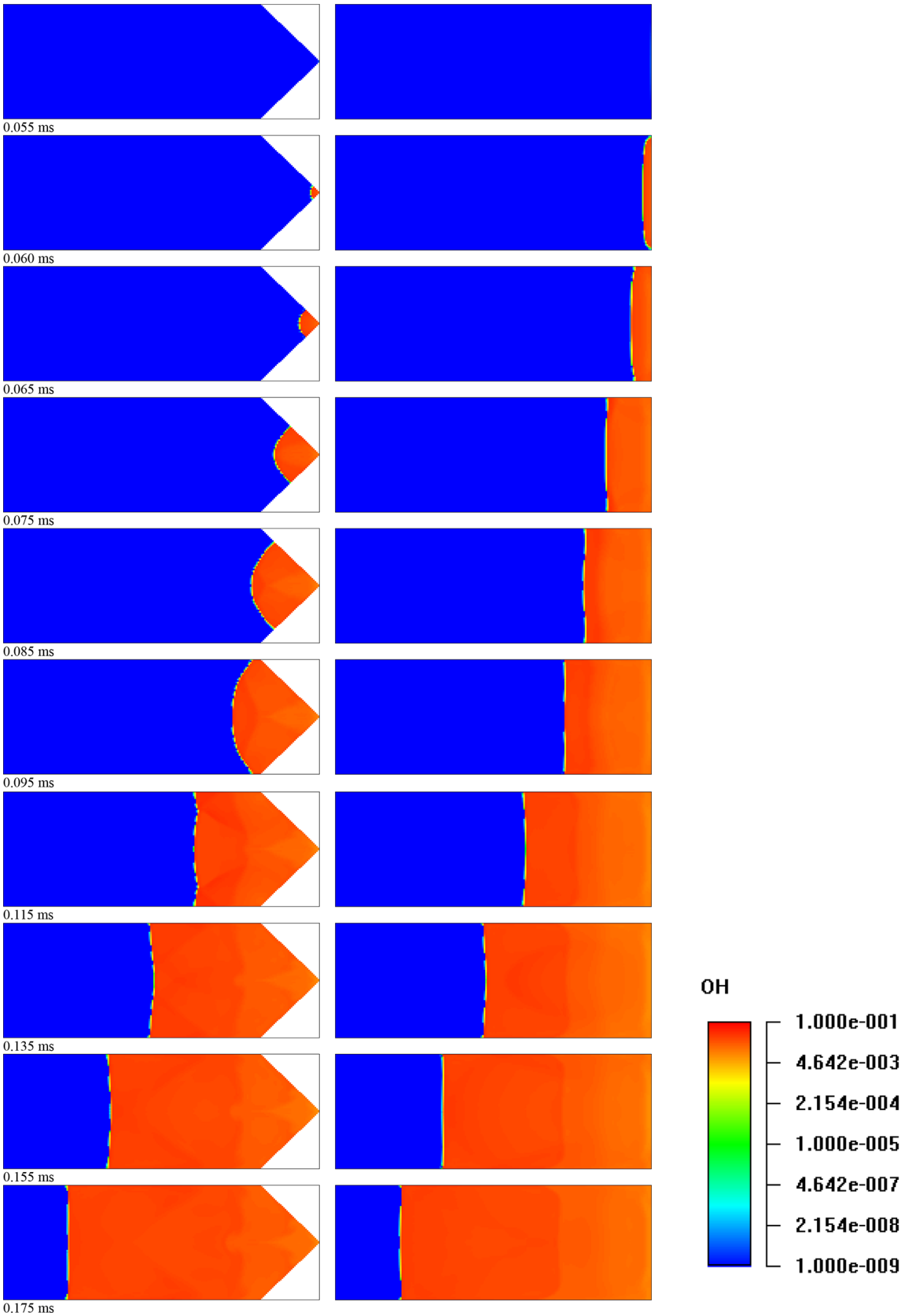

Fig. 6. Molar concentration of the OH radical evolution on the detonation onset in shock wave focusing on the reflection inside a wedge. *Oxy* meridional plane (left) and *Oxz* meridional plane (right); version WEDGE20R.

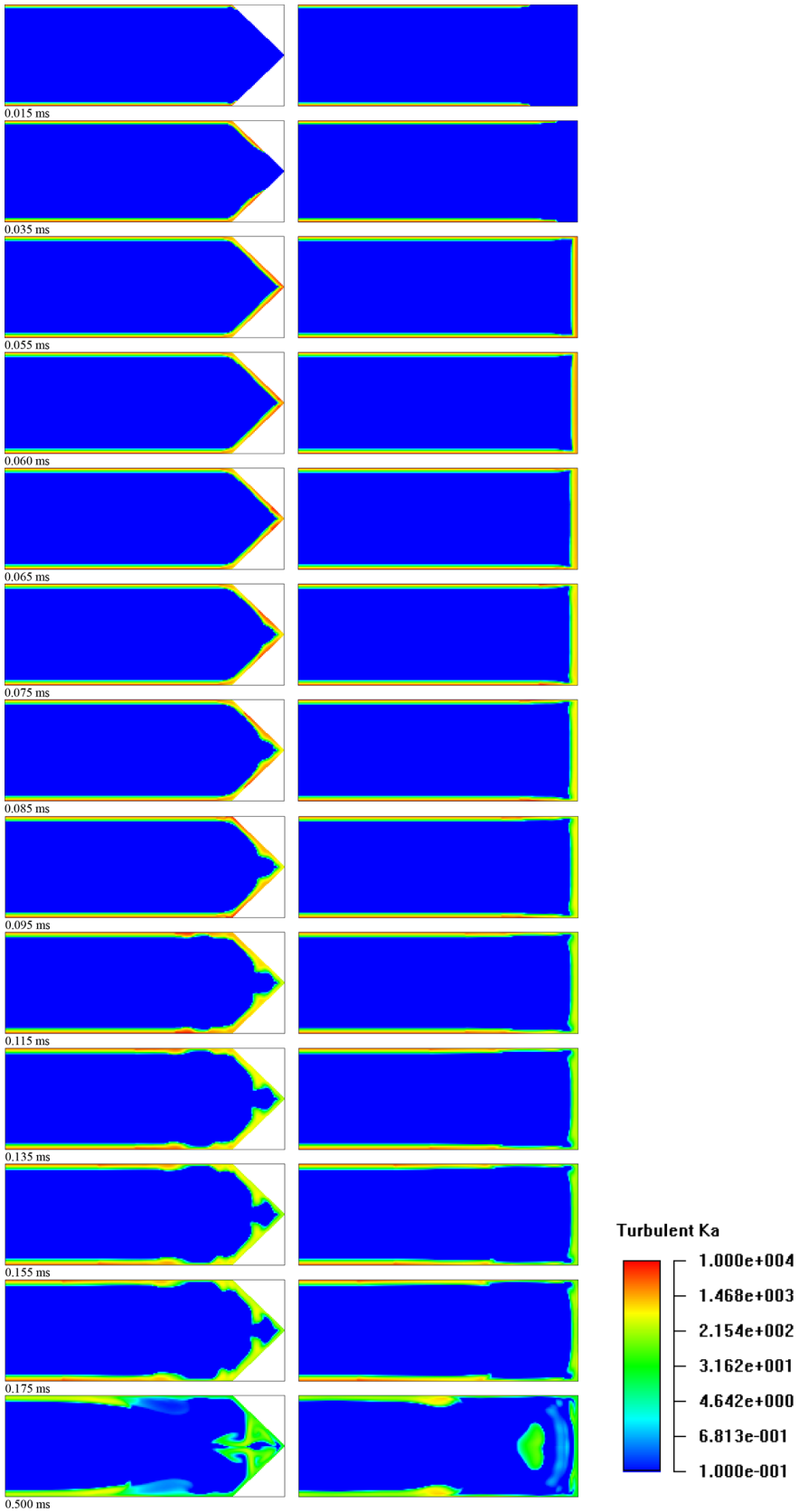

Fig. 7. Evolution of the turbulent kinetic energy K [J/kg] on the detonation onset in shock wave focusing on the reflection inside a wedge. Oxy meridional plane (left) and Oxz meridional plane (right); version WEDGE20R.

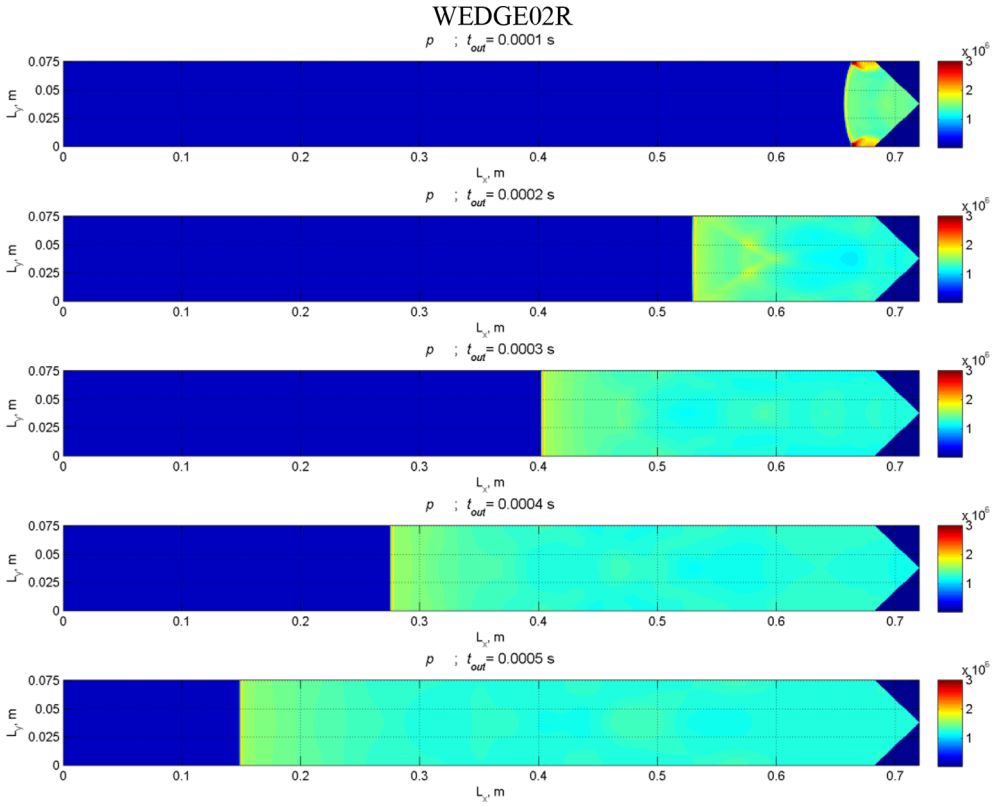

Fig. 8. Pressure fields for the shock wave reflection from a wedge in the cross-section Oxy for time moments 0.1, 0.2, 0.3, 0.4, 0.5 ms.

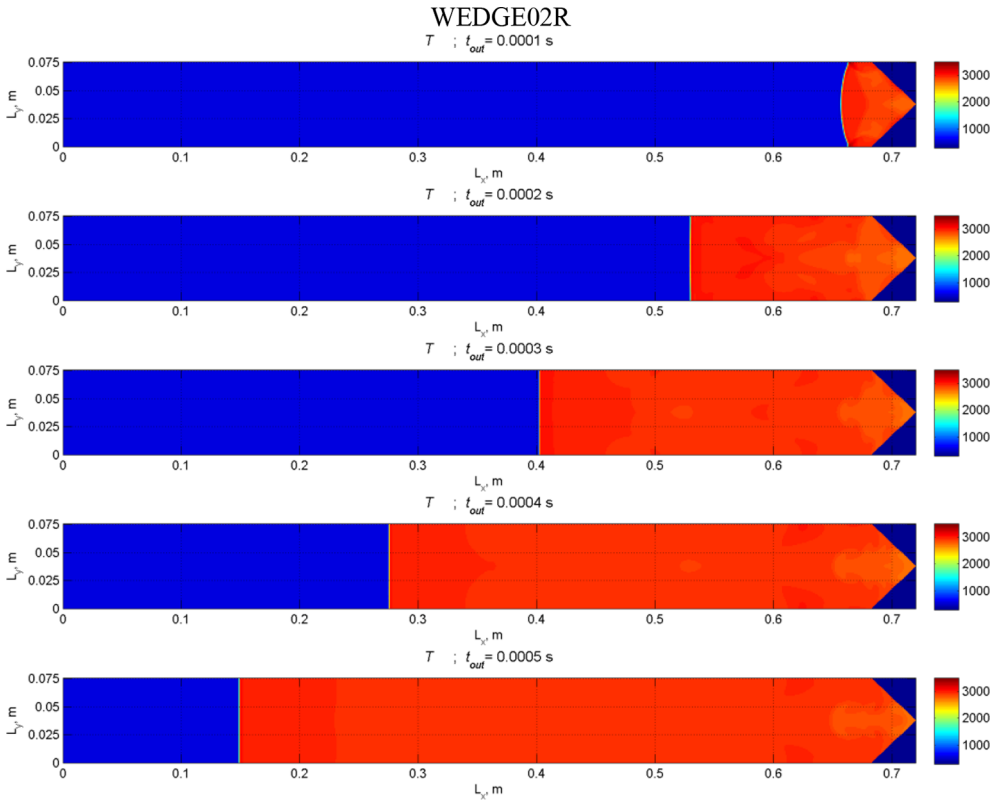

Fig. 9. Temperature fields for the shock wave reflection from a wedge in the cross-section Oxy for time moments 0.1, 0.2, 0.3, 0.4, 0.5 ms.

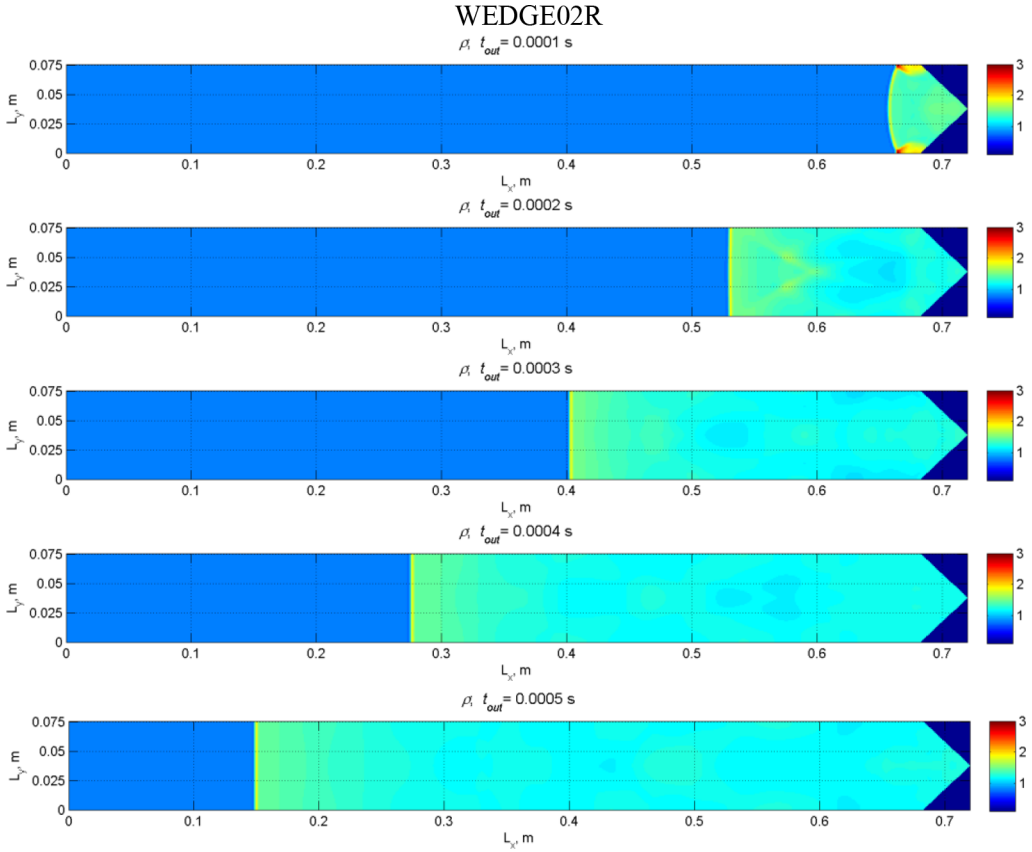

Fig. 10. Density fields for the shock wave reflection from a wedge in the cross-section Oxy for time moments 0.1, 0.2, 0.3, 0.4, 0.5 ms.

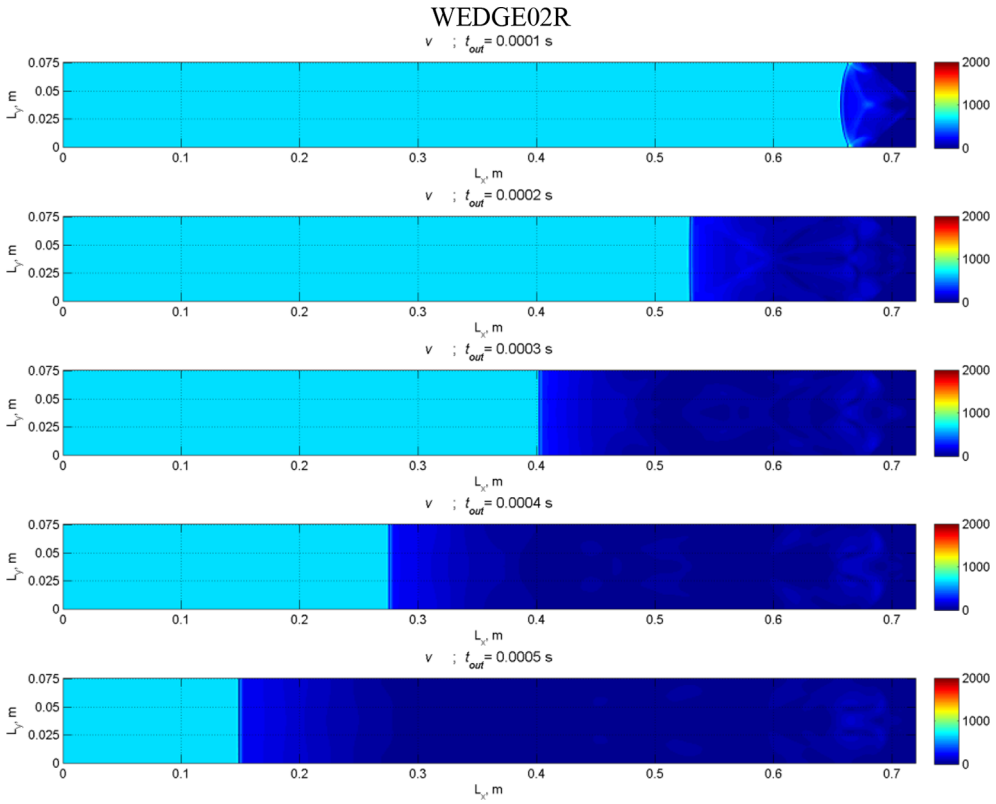

Fig. 11. Velocity modulus fields for the shock wave reflection from a wedge in the cross-section Oxy for time moments 0.1, 0.2, 0.3, 0.4, 0.5 ms.

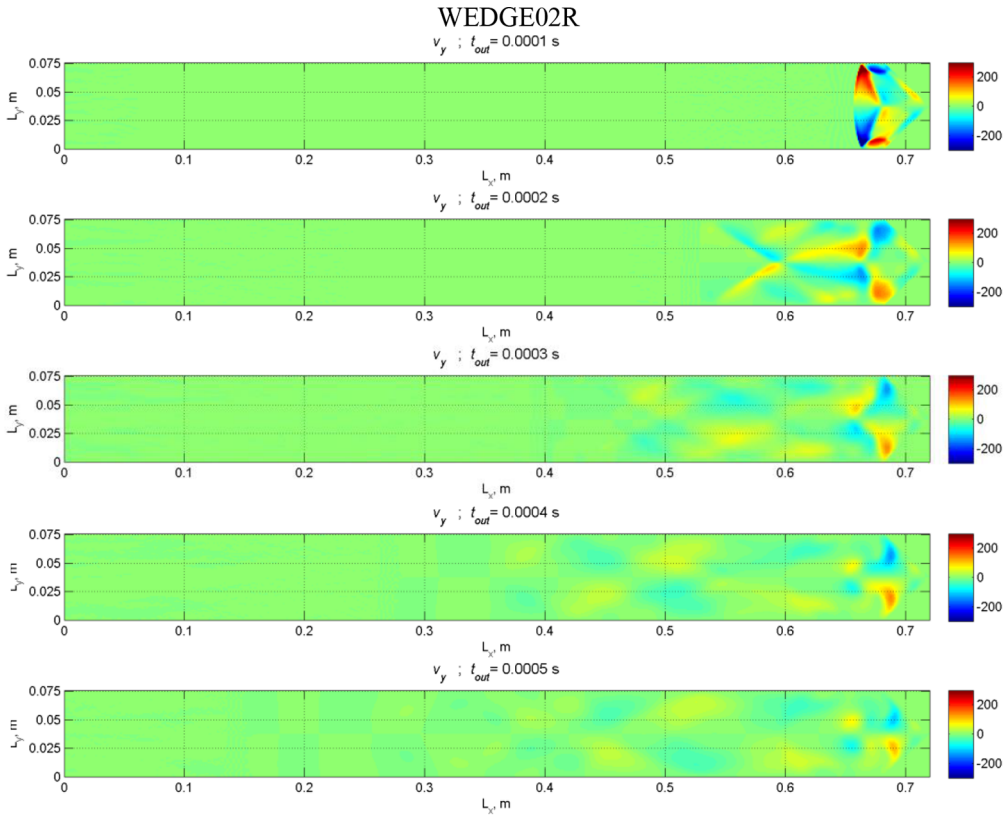

Fig. 12. Radial velocity fields for the shock wave reflection from a wedge in the cross-section Oxy for time moments 0.1, 0.2, 0.3, 0.4, 0.5 ms.

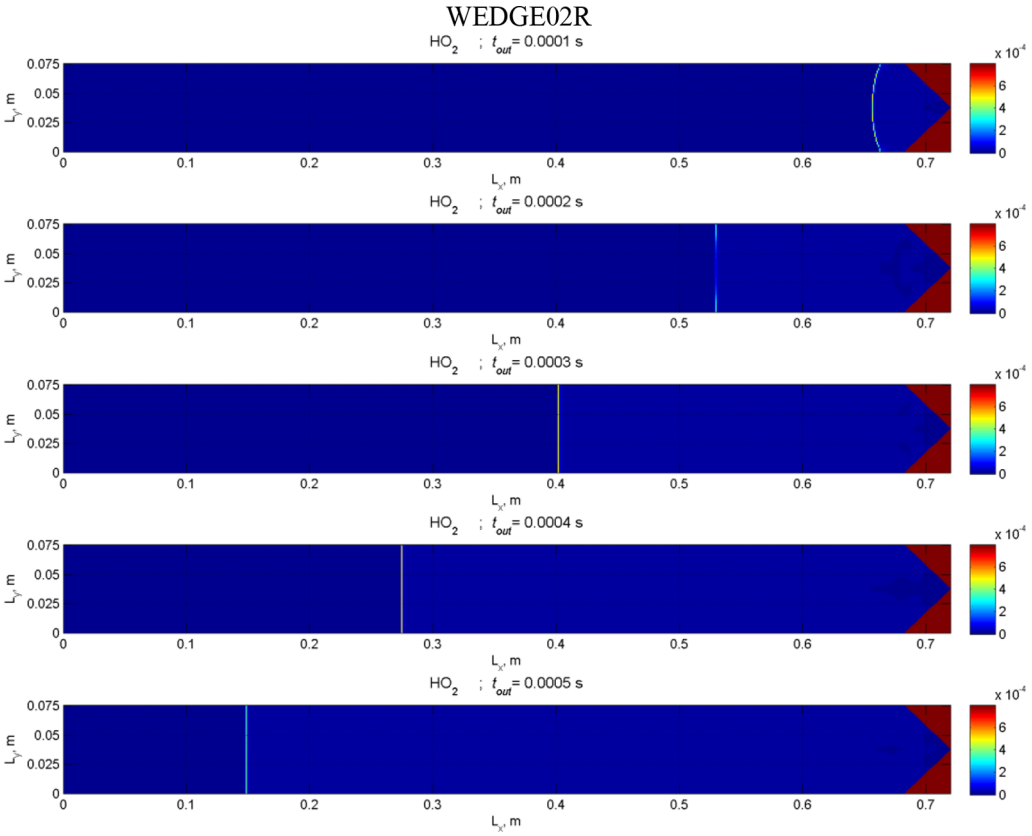

Fig. 13. Mass fraction of HO_2 radical fields for the shock wave reflection from a wedge in the cross-section Oxy for time moments 0.1, 0.2, 0.3, 0.4, 0.5 ms.

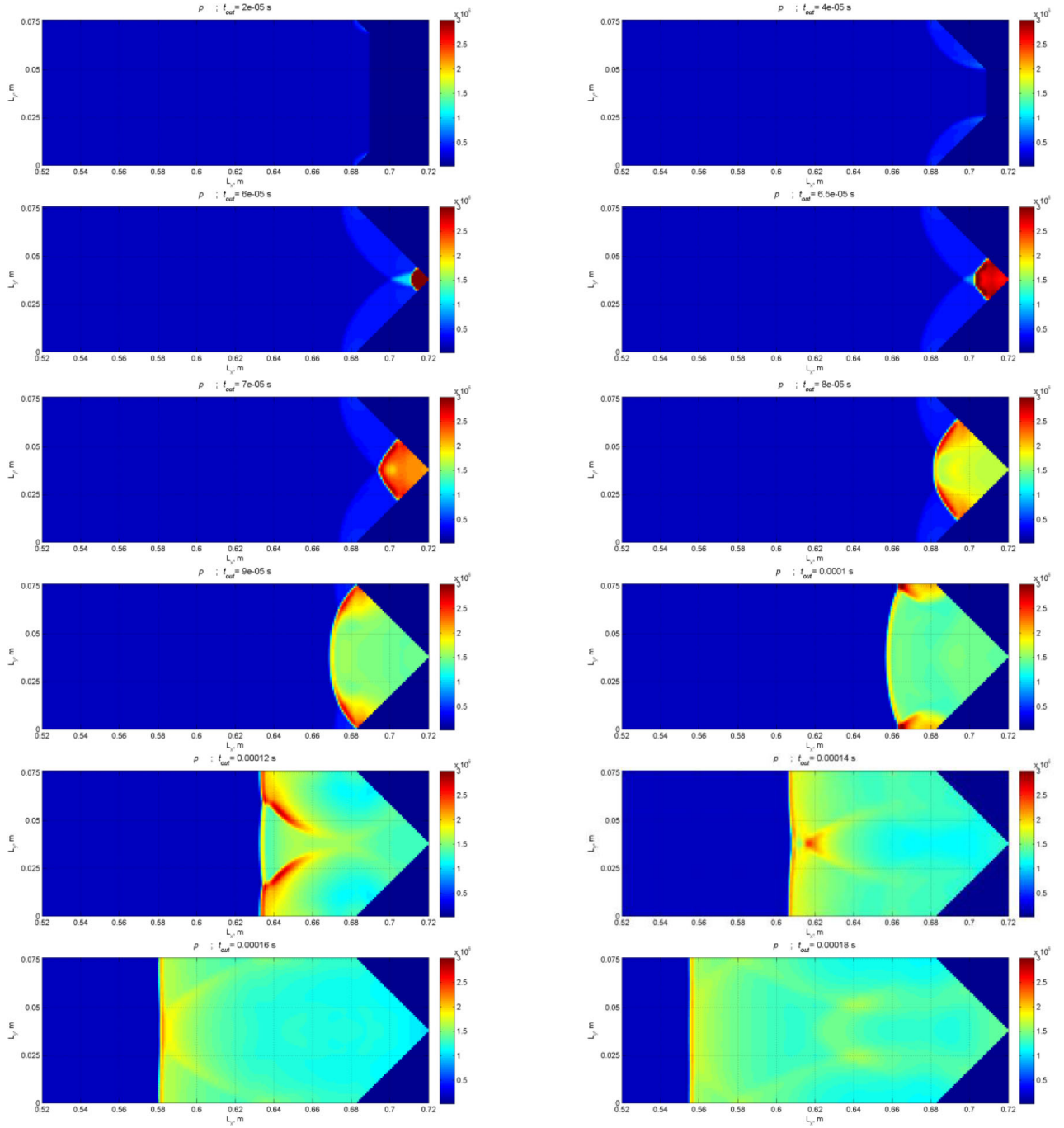

Fig. 14. Pressure fields for the shock wave reflection from a wedge in the cross-section Oxy for time moments 0.02, 0.04, 0.06, 0.065, 0.07, 0.08, 0.09, 0.10, 0.12, 0.14, 0.16, 0.18 ms; version WEDGE02R.

As seen from the figures, the onset of detonation due to focusing of a strong shock wave takes place via an overdriven detonation mode. Then the detonation wave slows down to a self-sustaining mode. The experimentally measured velocity, as well as that calculated using scheme 1, well coincide, but both diverge from the Chapman-Jouget velocity as a limit for the self-sustaining regime. On the other hand, numerical results based on scheme 2 have the Chapman-Jouget velocity as a limit. These differences can be explained by the effect of turbulence. In reflecting from a closed edge the detonation wave propagates through the disturbed and turbulized mixture, which possesses an additional turbulent kinetic energy delivered to the mixture by the incident shock wave. Due to this reason, the relative detonation wave velocity turns out to be higher than the Chapman-Jouget velocity calculated disregarding the initial mixture turbulization. Numerical model 2 does not take into account the turbulent energy production in the flow. Thus it provides the limiting velocity equal to the Chapman-Jouget value.

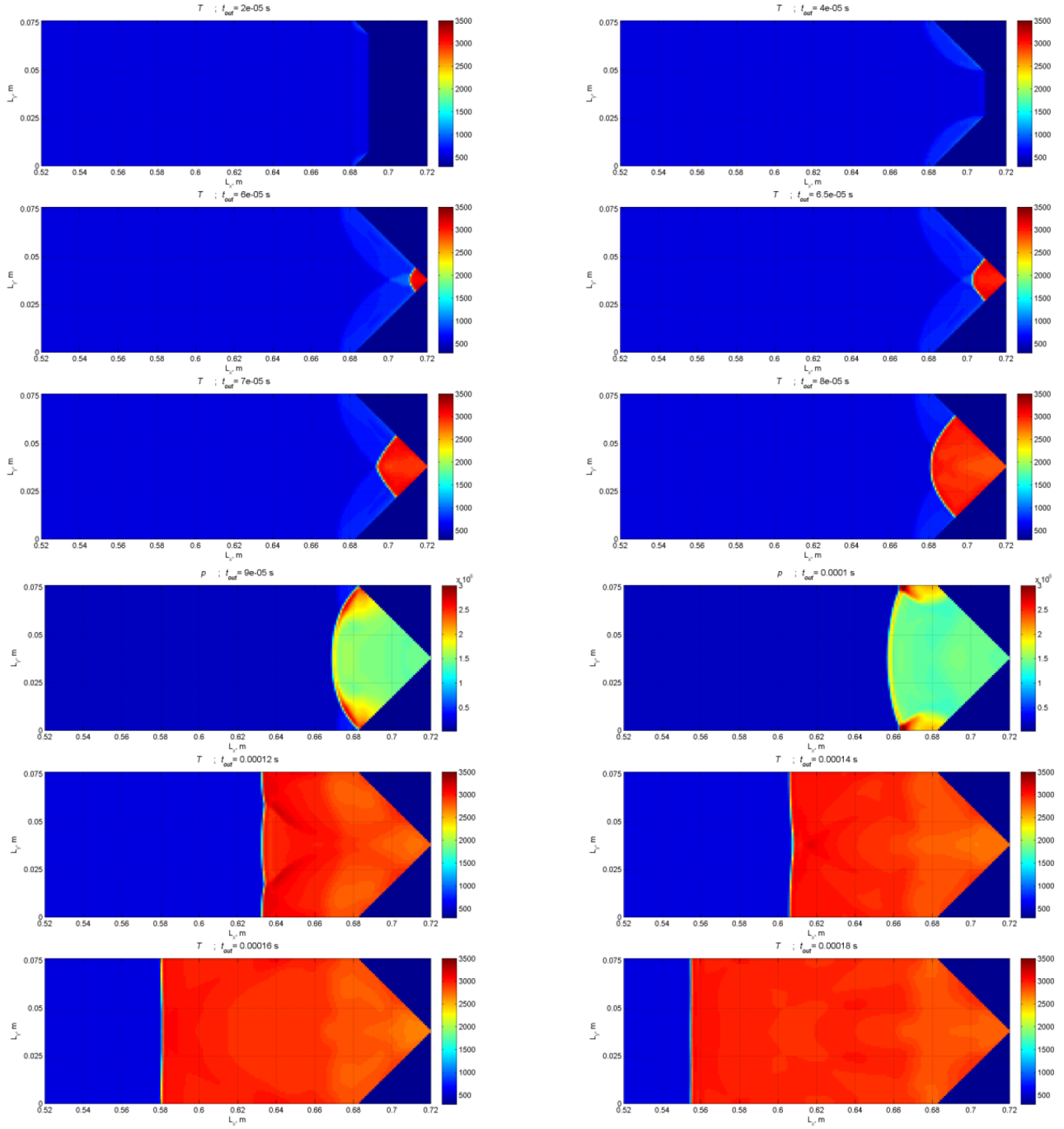

Fig. 15. Temperature fields for the shock wave reflection from a wedge in the cross-section Oxy for time moments 0.02, 0.04, 0.06, 0.065, 0.07, 0.08, 0.09, 0.10, 0.12, 0.14, 0.16, 0.18 ms; version WEDGE02R.

The results show that for the initial conditions under consideration the detonation onset does not take place. Shock wave focusing leads to the formation of an attenuating reflected shock wave. The coincidence of experimental and numerical results is very high.

The comparison of the results of numerical and physical experiments for different initial incident shock wave intensities showed that for relatively weak shock waves, when ignition behind the reflected shock wave does not occur, the difference of numerical and experimental data does not exceed 2.5%, while for incident shock waves of higher intensity, which lead to ignition after reflection and focusing, the velocity difference is around 4%. The transient regimes provide a larger difference between numerical and experimental results. It is seen from the figures, that the onset of detonation due to focusing of a strong shock wave takes place via an overdriven detonation mode. Then the detonation wave slows down to a self-sustaining mode. The experimentally measured velocity, as well as that calculated using scheme 1, well coincide, but both diverge

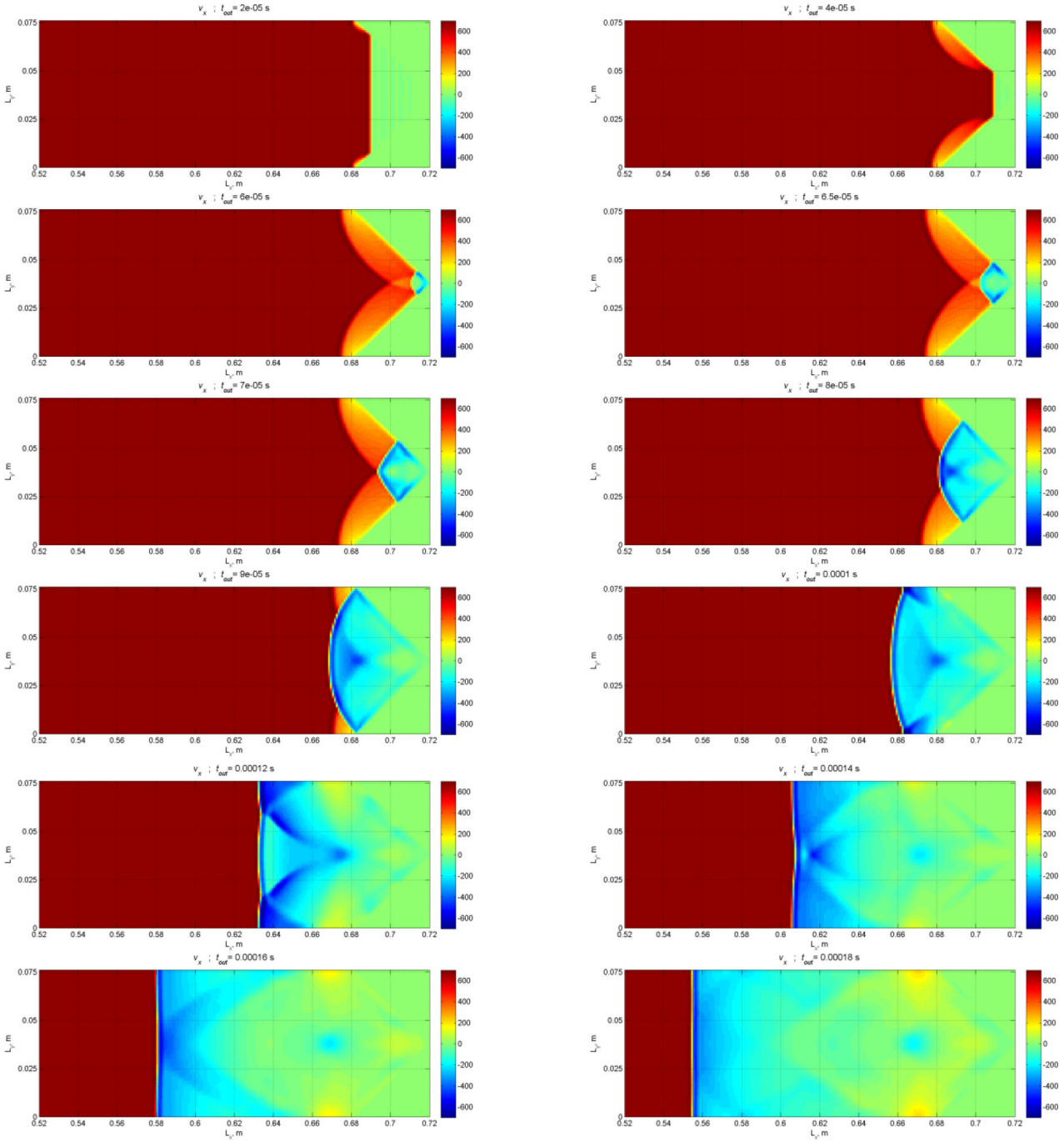

Fig. 16. Axial velocity fields for the shock wave reflection from a wedge in the cross-section *Oxy* for time moments 0.02, 0.04, 0.06, 0.065, 0.07, 0.08, 0.09, 0.10, 0.12, 0.14, 0.16, 0.18 ms; version WEDGE02R.

from the Chapman-Jouget velocity as a limit for the self-sustaining regime. On the other hand, numerical results based on scheme 2 have the Chapman-Jouget velocity as a limit. These differences can be explained by the effect of turbulence. In reflecting from a closed edge the detonation wave propagates through the disturbed and turbulized mixture, which possesses an additional turbulent kinetic energy delivered to the mixture by the incident shock wave. Due to this reason, the relative detonation wave velocity turns out to be higher than the Chapman-Jouget velocity calculated disregarding the initial mixture turbulization.

8 Conclusions

– Detonation initiation due to focusing of a shock wave reflected inside a cone was studied both numerically and experimentally.

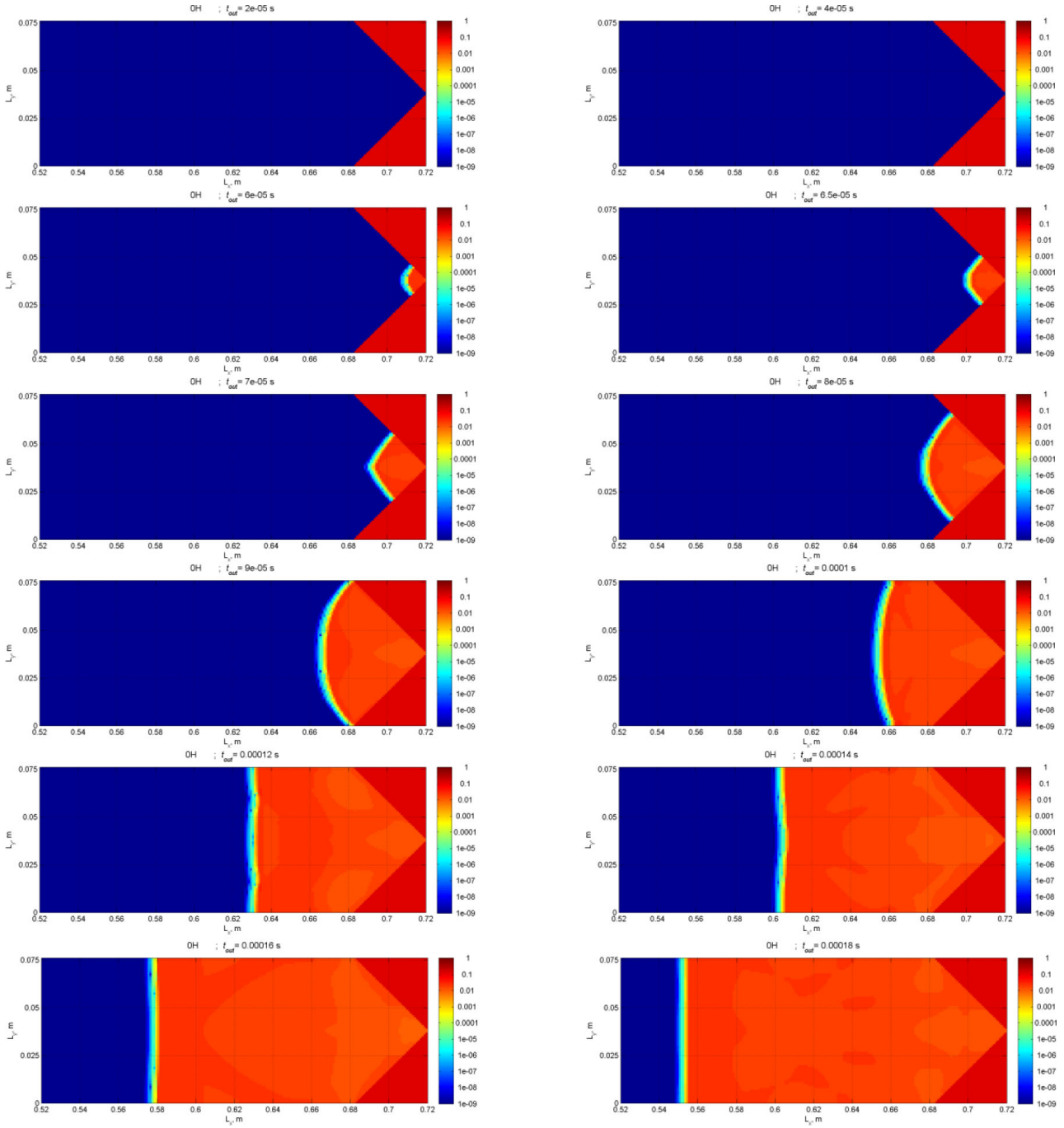

Fig. 17. Molar concentration of OH radical fields for the shock wave reflection from a wedge in the cross-section Oxy for time moments 0.02, 0.04, 0.06, 0.065, 0.07, 0.08, 0.09, 0.10, 0.12, 0.14, 0.16, 0.18 ms; version WEDGE02R.

– The comparison of the results made it possible to validate the developed 3D transient mathematical model of chemically reacting gas mixture flows incorporating hydrogen-air mixtures. The results of theoretical and numerical experiments made it possible to improve kinetic schemes and turbulence models.
– Several different flow scenarios were detected in the reflection of shock waves all being dependent on the incident shock wave intensity: reflection of a shock wave with lagging behind combustion zone, formation of a detonation wave in reflection and focusing, and intermediate transient regimes.
– The onset of detonation due to focusing of a strong shock wave takes place via an overdriven detonation mode. Then the detonation wave slows down to a self-sustaining mode.
– The experimentally measured velocity, as well as that calculated using scheme 1, well coincide, but both diverge from the Chapman-Jouget velocity as a limit for the self-sustaining regime. On the other hand, nu-

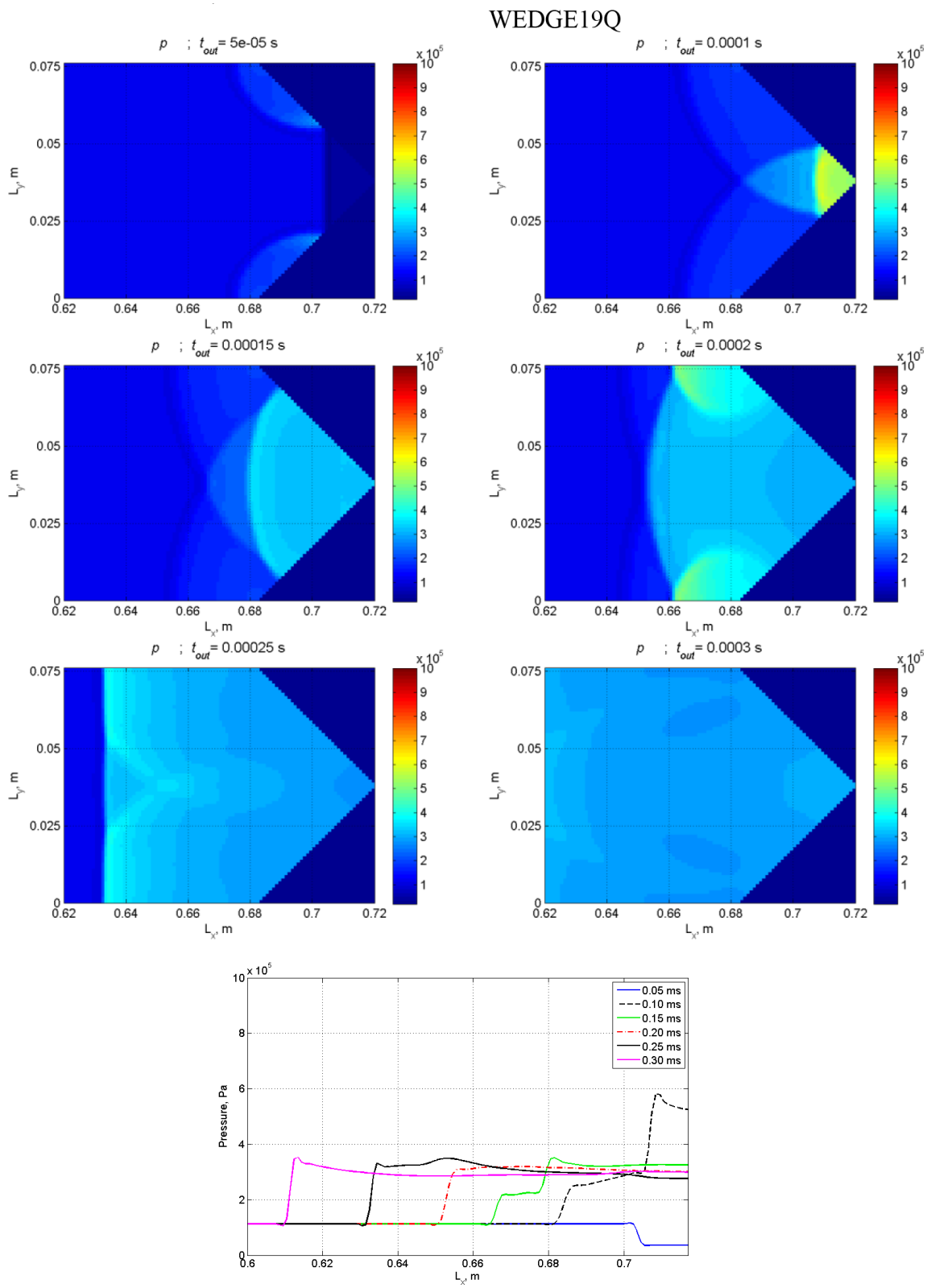

Fig. 18. Pressure fields (Pa) for the shock wave reflection from a wedge in the cross-section Oxy for time moments 0.05, 0.1, 0.15, 0.20, 0.25, 0.30 ms; version WEDGE19Q. Lower curves: pressure profiles along the Ox axis for the same times.

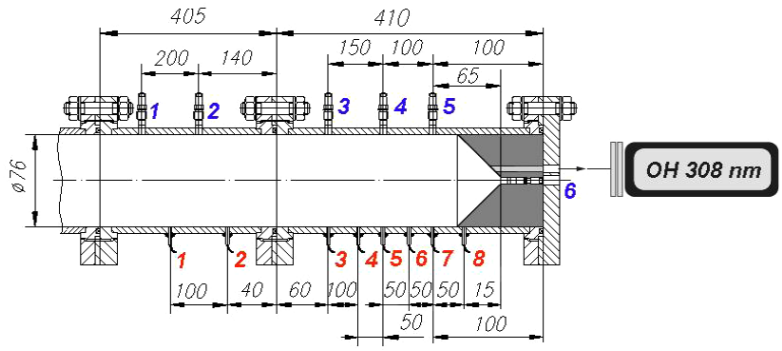

Fig. 19. The scheme of the end section of shock tube, wherein measurements were performed for shock waves focusing and reflection experiments. On top and in the center six pressure transducers are located. Opposite 8 ionization probes are located along the bottom wall, and the OH detector is located on the back wall close to the axis.

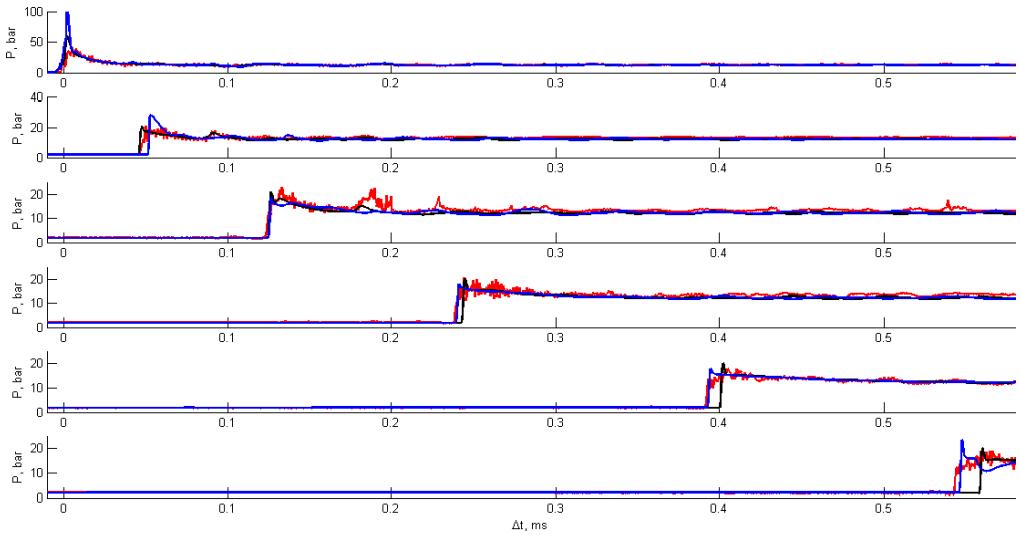

Fig. 20. Pressure-time history in control points after reflection and focusing of a shock wave in combustible hydrogen-air mixture: red curves, numbered 3: experiment; blue curves, numbered 1: numerical solution scheme 1; black curves, numbered 2: numerical solutions scheme 2. Version WEDGE02R. The figures from bottom to top correspond to the transducers numbered from 1 to 6 in fig. 19.

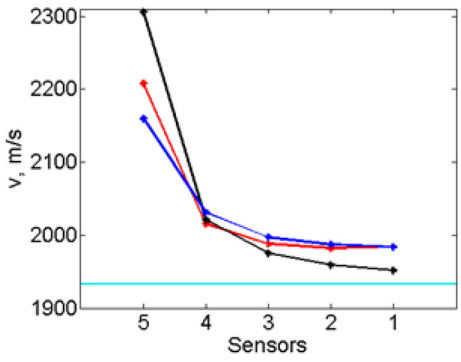

Fig. 21. Experimental results on the reflected shock wave mean velocity and its comparison with numerical simulations using codes based on scheme 1 and scheme 2, as well as its comparison with equilibrium calculations of the Chapman-Jouget detonation velocity: red curves, numbered 3: experiment; blue curves, numbered 1: numerical solution scheme 1; black curves, numbered 2: numerical solutions scheme 2; marine horizontal line: Chapman-Jouget velocity. Version WEDGE02R.

merical results based on scheme 2 have the Chapman-Jouget velocity as a limit. These differences can be explained by the effect of turbulence. In reflecting from a closed edge the detonation wave propagates through the disturbed and turbulized mixture, which possesses an additional turbulent kinetic energy delivered to the mixture by the incident shock wave. Due to this reason, the relative detonation wave velocity turns out to be higher than the Chapman-Jouget velocity calculated disregarding the initial mixture turbulization.

– The comparison of the results of numerical and physical experiments for different initial incident shock wave intensities showed that for relatively weak shock waves, when ignition behind the reflected shock wave does not occur, the difference of numerical and experimental data does not exceed 2.5%, while for incident shock waves of higher intensity, which lead to ignition after reflection and focusing, the velocity difference is around 4%. The transient regimes provide a larger difference between numerical and experimental results.

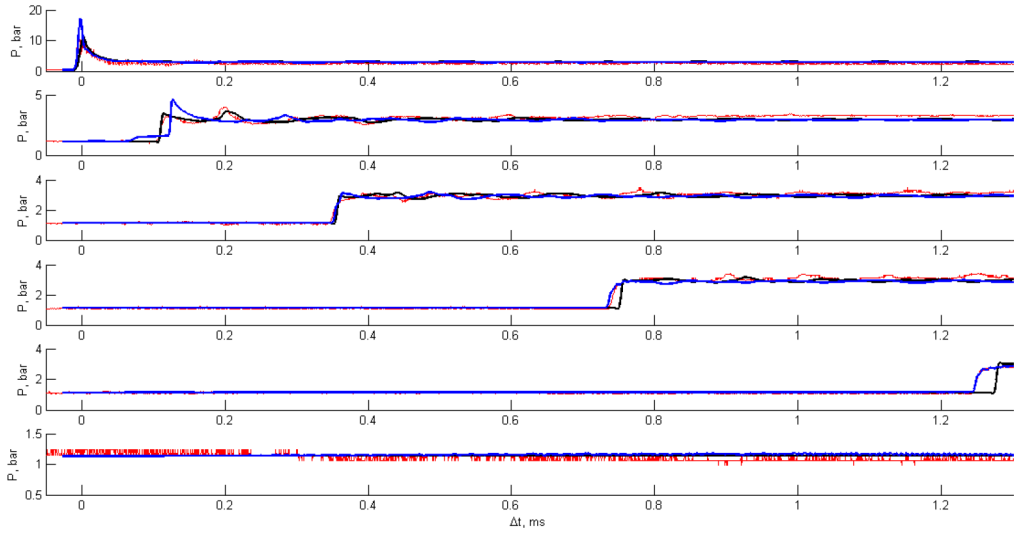

Fig. 22. Pressure-time history in control points after the reflection and focusing of the shock wave in the combustible hydrogen-air mixture: red curves, numbered 3: experiment; blue curves, numbered 1: numerical solution scheme 1; black curves, numbered 2: numerical solutions scheme 2. Version WEDGE19Q. The figures from bottom to top correspond to the transducers numbered from 1 to 6 in fig. 19.

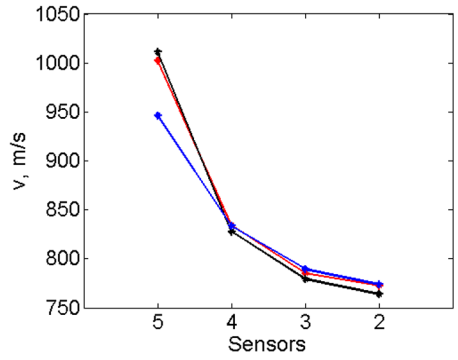

Fig. 23. Reflected wave velocity in control points after reflection and focusing of the shock wave in the combustible hydrogen-air mixture: red curves, numbered 3: experiment; blue curves, numbered 1: numerical solution scheme 1; black curves, numbered 2: numerical solutions scheme 2. Version WEDGE19Q.

Russian Foundation for Basic Research is acknowledged for financial support (Grant RFBR 17-03-00607).

Author contribution statement

N.N. Smirnov: general problem formulation, mathematical problem statement, analysis of numerical and experimental results, formulating conclusions. O.G. Penyazkov: developing the design of experiment and measuring systems, analysis of results. K.L. Sevrouk: performing experimental research, collecting and processing experimental data. V.F. Nikitin: developing software for numerical solution based on scheme 1 for universal systems. L.I. Stamov: developing software for numerical solution based on scheme 2 for hybrid systems. V.V. Tyurenkova: numerical data processing, comparing experimental and numerical results, analysis.

References

1. V.B. Betelin, N.N. Smirnov, V.F. Nikitin, Acta Astronaut. **109**, 269 (2015).
2. N.M. Marinov, W.J. Pitz, C.K. Westbrook, M. Hori, N. Matsunaga, *An Experimental and Kinetic Calculation of the Promotion Effect of Hydrocarbons on the NO-NO_2 Conversion in a Flow Reactor*, in *Proceedings of the Combustion Institute*, Vol. **27** (1998) pp. 389-396 (UCRL-JC-129372) UCRL-WEB-204236.
3. R.J. Kee, J.A. Miller, T.H. Jefferson, *Chemkin: a general-purpose, problem-independent, transportable Fortran chemical kinetics code package*, Sandia National Laboratories Report SAND80-8003 (1980).
4. S. Browne, J. Ziegler, J.E. Shepherd, *Numerical Solution Methods for Shock and Detonation Jump Conditions*, GALCIT Report FM2006.006, July 2004-Revised August 29, 2008.
5. S. Gordon, B.J. McBride, *Computer Program for Calculation of Complex Chemical Equilibrium Compositions and Applications I. Analysis*, NASA RP-1311, October 1994.
6. Z.G. Pozdnyakov, B.D. Rossi, *Handbook of Industrial Explosives and Means of Blasting* (M. Nedra, 1977).
7. E.J. Orlova, *Chemistry and Technology of High Explosives*, Textbook for universities, 3rd edition (L. "Chemistry", Leningrad branch, 1981).
8. U. Maas, J. Warnatz, Combus. Flame **74**, 53 (1988).
9. N.N. Smirnov, V.F. Nikitin, Int. J. Hydrog. Energy **39**, 1122 (2014).
10. N.N. Smirnov, V.B. Betelin, R.M. Shagaliev, V.F. Nikitin, I.M. Belyakov, Yu.N. Deryuguin, S.V. Aksenov, D.A. Korchazhkin, Int. J. Hydrog. Energy **39**, 10748 (2014).
11. N.N. Smirnov, V.B. Betelin, V.F. Nikitin, Yu.G. Phylippov, Jaye Koo, Acta Astronaut. **104**, 134 (2014).
12. NVIDIA CUDA, Programming Guide, 2016, `http://developer.nvidia.com/cuda-downloads`.
13. J.T. Ferziger, M. Peric, *Computational Methods for Fluid Dynamics*, 3d edition (Springer, 2002).

14. B. van Leer, J. Comput. Phys. **32**, 101 (1979).
15. M.-S. Liou, J. Comput. Phys. **129**, 364 (1996).
16. K. Fletcher, *Computational Methods in Fluid Dynamics*, in 2 volumes (Wiley, New York, 1991) English translation.
17. E.A. Novikov, *L-stable (4,2)-method of fourth order to solve hard problems*, Vestnik SamGU – Natural Science Series B, Vol. **8**(89) (2011) pp. 59–68.
18. B. Koren, *A robust upwind discretisation method for advection, diffusion and source terms*, in *Numerical Methods for Advection – Diffusion Problems*, edited by C.B. Vreugdenhil, B. Koren (Braunschweig, Vieweg, 1993) p. 117, ISBN: 3-528-07645-3.
19. N.N. Smirnov, V.F. Nikitin, Sh. Alyari-Shourekhdeli, Combus. Explos. Shock Waves **44**, 517 (2008).
20. N.N. Smirnov, V.F. Nikitin, Yu.G. Phylippov, J. Eng. Phys. Thermophys. **83**, 1287 (2010).
21. N.N. Smirnov, V.F. Nikitin, S. Alyari Shurekhdeli, J. Propuls. Power **25**, 593 (2009).
22. V.F. Nikitin, V.R. Dushin, Y.G. Phylippov, J.C. Legros, Acta Astronaut. **64**, 281 (2009).
23. Y. Wang, J. Wang, Y. Li, Y. Li, Int. J. Hydrog. Energy **39**, 11792 (2014).
24. A. Heidari, J.X. Wen, Int. J. Hydrog. Energy **39**, 21317 (2014).
25. Dan Wu, Yan Liu, Yusi Liu, Jianping Wang, Int. J. Hydrog. Energy **39**, 15803 (2014).
26. Yu.G. Phylippov, V.R. Dushin, V.F. Nikitin, V.A. Nerchenko, N.V. Korolkova, V.M. Guendugov, Acta Astronaut. **76**, 115 (2012).
27. Min-cheol Gwak, Younghun Lee, Ki-hong Kim, Jack J. Yoh, Int. J. Hydrog. Energy **40**, 3006 (2015).
28. Yuhui Wang, Jianping Wang, Int. J. Hydrog. Energy **40**, 7949 (2015).
29. F.A. Bykovskii, S.A. Zhdan, E.F. Vedernikov, A.N. Samsonov, A.S. Zintsova, Combust. Explos. Shock Waves **52**, 446 (2016).
30. F.A. Bykovskii, S.A. Zhdan, E.F. Vedernikov, Combust. Explos. Shock Waves **52**, 371 (2016).
31. F. Falempin, Tuijin Jishu/J. Propuls. Technol. **31**, 650 (2010).
32. F. Jouot, G. Dupré, A. Quilgars, I. Gökalp, E. Cliquet, Proc. Combust. Inst. **33**, 2235 (2011).
33. G. Roy, S. Frolov, K. Kailasanath, N. Smirnov (Editors), *Gaseous and Heterogeneous Detonations: Science to Applications* (ENAS Publ., Moscow, 1999) ISBN: 5-89055-016-0.
34. Gene M. Amdahl, Computer **46**, 38 (2013).
35. N.N. Smirnov, Acta Astronaut. **126**, 497 (2016).
36. G.A. Sod, J. Comput. Phys. **27**, 1 (1978).
37. R. Liska, B. Wendroff, SIAM J. Sci. Comput. **25**, 995 (2003).
38. N.N. Smirnov, V.B. Betelin, V.F. Nikitin, L.I. Stamov, D.I. Altoukhov, Acta Astronaut. **117**, 338 (2015).
39. N.N. Smirnov, V.F. Nikitin, L.I. Stamov, V.A. Nerchenko, V.V. Tyrenkova, Int. J. Comput. Methods **14**, 1750038 (2017).
40. N.N. Smirnov, O.G. Penyazkov, K.L. Sevrouk, V.F. Nikitin, L.I. Stamov, V.V. Tyurenkova, Acta Astronaut. **135**, 114 (2017).
41. V.V. Martynenko, O.G. Penyaz'kov, K.A. Ragotner, S.I. Shabunya, J. Eng. Phys. Thermophys. **77**, 785 (2004).
42. O.G. Penyazkov, K.A. Ragotner, A.J. Dean, B. Varatharajan, Proc. Combust. Inst. **30**, 1941 (2005).